

# Modeling the Multi-Band Afterglow of GRB 130831A: Evidence for a Spinning-Down Magnetar Dominated by Gravitational Wave Losses?

Q. Zhang<sup>1,2</sup>, Y. F. Huang<sup>3,4</sup>, H. S. Zong<sup>1,2,5</sup>

Received \_\_\_\_\_; accepted \_\_\_\_\_

---

<sup>1</sup>School of Physics, Nanjing University, Nanjing 210093, China; zonghs@nju.edu.cn

<sup>2</sup>Joint Center for Particle, Nuclear Physics and Cosmology, Nanjing 210093, China

<sup>3</sup>School of Astronomy and Space Science, Nanjing University, Nanjing 210093, China;  
hyf@nju.edu.cn

<sup>4</sup>Key Laboratory of Modern Astronomy and Astrophysics (Nanjing University), Ministry  
of Education, Nanjing 210093, China

<sup>5</sup>State Key Laboratory of Theoretical Physics, Institute of Theoretical Physics, CAS,  
Beijing, 100190, China

## ABSTRACT

The X-ray afterglow of GRB 130831A shows an “internal plateau” with a decay slope of  $\sim 0.8$ , followed by a steep drop at around  $10^5$  s with a slope of  $\sim 6$ . After the drop, the X-ray afterglow continues with a much shallower decay. The optical afterglow exhibits two segments of plateaus separated by a luminous optical flare, followed by a normal decay with a slope basically consistent with that of the late-time X-ray afterglow. The decay of the internal X-ray plateau is much steeper than what we expect in the simplest magnetar model. We propose a scenario in which the magnetar undergoes gravitational-wave-driven r-mode instability, and the spin-down is dominated by gravitational wave losses up to the end of the steep plateau, so that such a relatively steep plateau can be interpreted as the internal emission of the magnetar wind and the sharp drop can be produced when the magnetar collapses into a black hole. This scenario also predicts an initial X-ray plateau lasting for hundreds of seconds with an approximately constant flux which is compatible with observation. Assuming that the magnetar wind has a negligible contribution in the optical band, we interpret the optical afterglow as the forward shock emission by invoking the energy injection from a continuously refreshed shock following the prompt emission phase. It is shown that our model can basically describe the temporal evolution of the multi-band afterglow of GRB 130831A.

*Subject headings:* gamma-ray burst: individual (GRB 130831A) – ISM: jets and outflows – stars: neutron

## 1. INTRODUCTION

Gamma-ray bursts (GRBs) are the most energetic stellar explosions in the universe. These events produce a short prompt  $\gamma$ -ray emission followed by a multi-band afterglow that can be observed up to several years. The afterglows of GRBs are thought to originate from the synchrotron emission of shock-accelerated electrons produced by the interaction between the outflow and the external medium (Rees & Mészáros 1992; Mészáros & Rees 1993, 1997; Sari et al. 1998; Huang et al. 1999; Chevalier & Li 2000). Before the launch of the *Swift* satellite (Gehrels et al. 2004), the afterglows were often observed to decay as a power law with time ( $F_\nu \propto t^{-1} - t^{-2}$ ) and have a power-law spectrum ( $F_\nu \propto \nu^{-0.9 \pm 0.5}$ ) which can be well explained by the synchrotron radiation from the external forward shock (Kumar & Zhang 2015). However, *Swift* observations have shown evidence of more complex phenomena during the afterglow phase, such as X-ray flares (Falcone et al. 2007; Chincarini et al. 2010; Margutti et al. 2011) and the shallow decay phase (or the so-called “plateau”; Nousek et al. 2006; O’Brien et al. 2006; Zhang et al. 2006; Evans et al. 2009; Margutti et al. 2013), which challenge the standard afterglow models (Sari et al. 1998; Chevalier & Li 2000).

A good fraction of *Swift* GRB afterglows exhibit an X-ray plateau that lasts for  $10^3 - 10^4$  s with a slope of  $\sim 0.3$ , followed by a normal or steeper decay with a slope of  $\sim 1 - 2$  (Nousek et al. 2006; Zhang et al. 2006; Evans et al. 2009; Racusin et al. 2009; Grupe et al. 2013; Margutti et al. 2013). Since this type of plateau can be typically interpreted as afterglow emission from the external shock in the context of the energy injection model (Zhang et al. 2006), it is often referred to as an “external plateau”, though some internal dissipation processes (e.g., Ghisellini et al. 2007) may also account for this phenomenon. In a small subset of *Swift* GRB afterglows, observations have shown an X-ray plateau followed by a very sharp drop with a decay slope steeper than 3, sometimes approaching

$\sim 9 - 10$  (Liang et al. 2007; Troja et al. 2007; Lyons et al. 2010; Rowlinson et al. 2010, 2013; Lü & Zhang 2014; Lü et al. 2015). Such a steep decay cannot be accommodated in any external forward shock model<sup>1</sup>, and the entire plateau emission is usually attributed to the internal dissipation of a central engine wind. Clues for such “internal plateaus” have been found in several short GRBs (Rowlinson et al. 2013), but are indicated in only a small portion of long GRBs (Troja et al. 2007; Lyons et al. 2010). Two types of GRB central engines have been widely studied in the literature: a hyper-accreting stellar-mass black hole (e.g., Popham et al. 1999; Narayan et al. 2001; Lei et al. 2013), and a rapidly spinning, strongly magnetized neutron star or “millisecond magnetar” (Usov 1992; Thompson 1994; Dai & Lu 1998; Wheeler et al. 2000; Zhang & Mészáros 2001; Metzger et al. 2008; Bucciantini et al. 2012). Within the scenario of a millisecond magnetar, the internal plateau can be interpreted as the internal emission of a spinning-down magnetar which collapses into a black hole at the end of the plateau (Troja et al. 2007; Rowlinson et al. 2010; Zhang 2014). Since the GRB outflow still produces X-ray afterglow by the external shock during the internal plateau phase, it is expected to emerge once the X-ray emission from the magnetar wind drops below the external component. So far, this has been seen clearly in the X-ray afterglow of the long GRB 070110 (Troja et al. 2007).

GRB 130831A (De Pasquale et al. 2016) is another event that exhibits a superposition of external and internal emission in the X-ray afterglow. The X-ray light curve (LC) shows a shallow decay with a slope of  $\sim 0.8$ , followed by a sharp drop at about  $10^5$  s with a slope of  $\sim 6$ . After the drop, the X-ray afterglow continues with a much shallower decay. Such a steep drop indicates that the shallow decay phase must be of “internal origin” (De Pasquale et al. 2016). However, the slope of this internal plateau is much steeper than

---

<sup>1</sup>From this point onwards, we use “external shock” as a synonym of “forward shock”, and we do not consider reverse shock emission.

the usually observed, and cannot be explained by the simplest magnetar model which predicts a plateau with approximately constant flux. De Pasquale et al. (2016) proposed a more elaborate model of the magnetar spin-down, in which the magnetic field is assumed to decay as the spin period increases (Metzger et al. 2011). This is possible but detailed numerical calculations are needed to test this possibility.

In this paper, we propose a new scenario to explain the internal X-ray plateau of GRB 130831A. In our model, the nascent magnetar could undergo some nonaxisymmetric stellar instabilities (e.g., r-mode instability; Andersson 1998; Friedman & Morsink 1998), leading to strong gravitational wave (GW) losses which would affect the magnetar’s spin-down (Corsi & Mészáros 2009). In the context of r-mode instability (Sá & Thomé 2005, 2006; Yu et al. 2010), if the gravitational braking timescale ( $\tau_g$ ) is much smaller than the magnetic braking timescale ( $\tau_m$ ), the spin-down would be first dominated by GW losses and the luminosity of the magnetar wind can be regarded as a constant within a timescale comparable to  $\tau_g$  ( $\sim$  a few  $\times 10^2$  s for a neutron rotating with the Keplerian frequency; Sá & Thomé 2005). After that, the spin of the magnetar would be remarkably decelerated and the luminosity of the wind evolves as  $L_w \propto t^{-4/5}$ . At later times, the spin-down would be eventually dominated by the magnetic dipole radiation and  $L_w$  decays as  $t^{-2}$ . During the spin-down process, the magnetar could collapse into a black hole and a steep drop of the wind luminosity would be observed. We test this scenario using the multi-band afterglow of GRB 130831A in this work.

In addition, GRB 130831A has a well-sampled and multi-band optical afterglow. The optical LCs exhibit two segments of plateaus separated by a luminous optical flare, followed by a normal decay with a slope basically consistent with that of the late-time X-ray afterglow (De Pasquale et al. 2016). De Pasquale et al. (2016) interpreted the afterglow after the flare as the forward shock (FS) emission in the context of the standard

afterglow models by requiring the ejecta decelerating at  $\sim 4$ ks. However, their model cannot explain the initial optical plateau before  $\sim 500$  s. To solve this problem, we assume that these two plateaus have the same FS origin and are produced by an energy injection process (Zhang et al. 2006). We will show in Section 3 that this energy injection cannot be supplied by the magnetic wind (Dai & Lu 1998; Zhang & Mészáros 2001), since the wind luminosity has a negligible contribution to the FS emission. We also assume that the magnetar wind emission contributes negligibly in the optical band and we invoke the model of Sari & Mészáros (2000) to explain the entire optical afterglow. In this case, the energy injection is produced by a continuously refreshed shock following the prompt emission phase (Rees & Mészáros 1998).

Our paper is organized as follows. We summarize the observational facts of GRB 130831A and refit the afterglow LCs in Section 2. In Section 3, we model the external afterglow by invoking the energy injection model, and interpret the internal X-ray afterglow as the magnetar wind emission produced by the spin-down process dominated by GW losses. In Section 4, we compare our theoretical afterglow LCs with observations. Finally, we present our conclusions and give a brief discussion in Section 5. Throughout the paper, the convention  $F_\nu \propto \nu^{-\beta} t^{-\alpha}$  is followed, and we use the standard notation  $Q_x = Q/10^x$  with  $Q$  being a generic quantity in cgs units. We assume a concordance cosmology with  $H_0 = 70 \text{ km s}^{-1} \text{Mpc}^{-1}$ ,  $\Omega_M = 0.27$  and  $\Omega_\Lambda = 0.73$  (Jarosik et al. 2011). All the errors are given at the  $1\sigma$  confidence level (CL).

## 2. OBSERVATIONAL FACTS

GRB 130831A triggered the *Swift* Burst Alert Telescope (BAT; Barthelmy et al. 2005) at  $T_0 = 13:04:16.54$  UT on 2013 August 31 and was also observed by *Konus-Wind* onboard the *WIND* spacecraft. The light curve in the 15 – 350 keV energy range shows a main pulse

with a fast rise and exponential decay (FRED) shape, followed by some extended emission that lasts until  $T_0 + 41$  s. The measured duration of  $T_{90}$  in the 15 – 350 keV band is  $30.2 \pm 1.4$  s (De Pasquale et al. 2016). The time-averaged spectrum between 20 keV and 15 MeV can be fitted by a Band function (Band et al. 1993) with the peak energy  $E_p = 55 \pm 4$  keV, the low-energy photon index  $\alpha = -0.61 \pm 0.06$  and the high-energy photon index  $\beta = -2.3 \pm 0.3$ . The fluence between 20 keV and 10 MeV is  $(7.6 \pm 0.2) \times 10^{-6}$  erg cm $^{-2}$  (Golenetskii et al. 2013). With a redshift of  $z = 0.479$  (Cucchiara & Perley 2013), this corresponds to an isotropically equivalent energy  $E_\gamma = 1.06 \times 10^{52}$  erg in the 1 – 10000 keV rest-frame energy band (De Pasquale et al. 2016).

## 2.1. X-Ray Afterglow

The X-ray Telescope (XRT; Burrows et al. 2005) began observations of GRB 130831A 125.8 s after the BAT trigger, and monitored the source until 2013 September 14. The X-ray afterglow of GRB 130831A was also observed by *Chandra* at  $T_0 + 16.6$  d and  $T_0 + 33.1$  d (De Pasquale et al. 2016). As shown in Figure 1, the X-ray LC shows an initial fast decay ending at about 200 s, then it gives way to a shallower decay up to about 100 ks. After that, the flux drops quickly, then evolves slowly again at around 200 ks. In addition, there is a X-ray flare between about 500 and 900 s.

De Pasquale et al. (2016) fit the X-ray afterglow with the sum of an initial power law (PL), a broken power law (BPL) and a final PL together with a Gaussian function. They found that the plateau between 0.3 and 100 ks can be well described by a single PL with slope of  $\sim 0.8$ . It is not clear how this plateau evolves before 0.3 ks. According to our GW radiation dominated magnetar model, there should be an initial plateau within hundreds of seconds. However, the X-ray data show no evidence of such an initial plateau. One possibility is that this short plateau indeed exists but ends before  $\sim 300$  s and is buried by

the initial steep decay of the X-ray afterglow. Therefore, we give a physically motivated fit to the X-ray afterglow based on our new considerations. We use the data of 0.3 – 10 keV unabsorbed X-ray flux produced by an automatic analysis procedure (Evans et al. 2007, 2009). We focus on the data before  $\sim 10^5$  s and fit the LC with an initial PL, a BPL and a Gaussian function. We fix the initial decay index of the BPL as zero which is predicted by our magnetar model. The main purpose of our fit here is to draw some key information from the observational data, such as the time of light curve breaks, the flux level, the power-law indices, etc. We use the Origin software (Version 8.5<sup>2</sup>) to perform a least-square fit to obtain the model parameters. Figure 1 shows our fit of the X-ray afterglow before  $10^5$  s. The main fitting parameters are listed in Table 1. We note that our parameter values are basically consistent with those given by De Pasquale et al. (2016) except that we have two extra parameters, i.e., the flux and the break time ( $\sim 270$  s) of the initial short plateau. The main difference between our results and those of De Pasquale et al. (2016) is that we have introduced an initial plateau in our fit, though such a short plateau cannot be identified just from the data.

For late X-ray afterglow after  $\sim 100$  ks, we adopt the results of De Pasquale et al. (2016): the best-fitting slope of the steep drop is  $6.8_{-1.5}^{+2.0}$  and the late shallow decay index is  $1.11_{-0.29}^{+0.22}$ . In addition, the X-ray spectrum between 9 and 132 ks can be modeled with an absorbed PL, which yields the spectral index  $\beta_X = 0.77 \pm 0.07$  and the host absorbing column density  $N_H = 6.8_{-3.1}^{+3.3} \times 10^{20} \text{cm}^{-2}$  (De Pasquale et al. 2016).

---

<sup>2</sup>[www.originlab.com](http://www.originlab.com)



## 2.2. Optical Afterglow

The optical afterglow of GRB 130831A was observed by *Swift*/UVOT (Roming et al. 2005) from 114 s after the trigger (Hagen et al. 2013), and it was also monitored by several ground telescopes and IKI Network for Transients, such as the Reionization and Transients Infra-Red camera (RATIR; Butler et al. 2012), Skynet (Reichart et al. 2005) and the International Scientific Optical-Observation Network (ISON; Molotov et al. 2008; Pozanenko et al. 2013). De Pasquale et al. (2016) gave a detailed study of the multi-color afterglow ranging from the infrared to ultraviolet bands, while the data analysis of SN 2013fu that is associated with this burst can be found in Cano et al. (2014).

The optical LCs show an initial short plateau (in the  $U$  band) that lasts until  $\sim 500$  s, followed by a bump peaking at around 730 s. This optical bump is basically concurrent with the X-ray flare and evolves rapidly. After the bump, there is another plateau that in turn gives way to a steeper decay at  $\sim 5$  ks (De Pasquale et al. 2016). De Pasquale et al. (2016) fit the LCs between 3.5 and 15 ks with a BPL. They assumed that the observed bumps at  $\sim 730$  s are optical flares since they peak at the same time as the X-ray flare and have a rapid temporal behavior, while they have not taken into account the early data (before  $\sim 3.5$  ks) in their fit.

Our main interest here is the origin of the initial optical plateau. As stated in Section 1, it is natural to assume the initial plateau is produced by the external shock, and has the same origin as the later plateau (between 3.5 and 5 ks). In this case, a fit including the early data (especially for the  $V$  band) is necessary. Therefore, we refit the optical afterglow before  $\sim 16$  ks (Figure 2). We fit the  $V, B$  and unfiltered bands with two BPLs. For the  $R$  and  $I$  bands, we fit the decaying segment of the flare with a PL and fit the post-flare data with a BPL. For the  $U$  band, we fit only the initial plateau with a PL. We perform the same fitting procedure as that in Section 2.1. As seen from Table 2, our fit gives relatively high

$\chi^2/dof$ . Such high  $\chi^2/dof$  are also given by De Pasquale et al. (2016), they are mainly due to some “wiggles” of the densely sampled LCs in this phase. Comparing the parameters with those of De Pasquale et al. (2016), we have similar break times at  $\sim 5$  ks, while the decay indices ( $\sim 1.32 - 1.55$ ) are slightly shallower than theirs ( $\sim 1.45 - 1.82$ ). However, the biggest difference lies in the decay slopes of the plateaus. For the  $V$  and  $U$  bands, our obtained slopes ( $\sim 0.2$ ) are significantly smaller than theirs ( $\sim 0.8$ ), since we have included the early data before  $\sim 3$  ks. While for other bands, we even give negative slopes. It is not unexpected since the superposition of a decaying optical flare and a rising peak can produce a plateau-like feature. This is consistent with the model of De Pasquale et al. (2016), in which the late plateau results from the combination of the decaying optical flare and the rising of the FS peak. However, their model cannot explain the initial short plateau. Since we assume these two plateaus are of the same origin, a plateau slope of  $\sim 0.2$  is preferred. For the post-plateau decay slope, we use the value of  $\sim 1.59$  given by De Pasquale et al. (2016) since they made a more in-depth analysis in this phase. In addition, The spectral energy distribution (SED) with the optical and X-ray data at 2 days gives a spectral index  $\beta_{\text{OX}} = 1.03^{+0.05}_{-0.04}$  and a small or absent amount of host-galaxy reddening  $E(B - V) = 0.02 \pm 0.01$  mag (De Pasquale et al. 2016; Cano et al. 2014).

### 3. MODEL

#### 3.1. Afterglow of External Origin

The optical afterglow of GRB 130831A shows a long plateau before  $\sim 5$  ks, a similar plateau must have appeared in the external component of the X-ray afterglow in this period if we assume the X-ray and the optical emissions lie on the same spectral segment throughout the afterglow observations. Theoretically, several models have been proposed to interpret the afterglow plateau (e.g., Zhang & Mészáros 2001; Sari & Mészáros

2000; Eichler & Granot 2006; Ioka et al. 2006; Ghisellini et al. 2007; Shao & Dai 2007; Uhm & Beloborodov 2007), some of them can even explain the chromatic breaks in GRB afterglows (Ghisellini et al. 2007; Uhm & Beloborodov 2007). For the simplest case that the X-ray and the optical LCs have achromatic behaviors, the energy injection models are usually adopted and the plateau phase can be produced by a significant continuous energy injection into the decelerating forward shock. There are at least two possible physical origins for the energy injection, depending on whether the central engine is long or short lived (Zhang et al. 2006): (i) The central engine is long lived and the luminosity is assumed to evolve as  $L(t) \propto t^{-q}$  with  $q < 1$ . A specific case, corresponding to  $q = 0$ , is that the energy injection is from the spin-down of a millisecond pulsar or magnetar (Dai & Lu 1998; Zhang & Mészáros 2001). (ii) The engine is short lived (i.e., with duration comparable to that of the prompt phase) and is assumed to produce shells with a steep power-law distribution of Lorentz factors and most of the system’s energy is carried by the slower material (Rees & Mészáros 1998; Sari & Mészáros 2000). Both scenarios interpret the plateau as afterglow emission from a continuous refreshed shock, which requires the injected energy largely exceeding the initial kinetic energy of the ejecta.

For GRB 130831A, the possibility that the energy injection is from the spin-down of a magnetar can be excluded. To show that, we give a rough estimate. The initial plateau luminosity of the X-ray afterglow is  $\sim 10^{47}$  erg s $^{-1}$  (see table 1). We assume that the efficiency of converting the magnetic dipole emission into X-ray radiation is  $\sim 0.1$ , then the isotropically equivalent luminosity of the magnetar wind is  $\sim 10^{48}$  erg s $^{-1}$ . The injected energy increases as  $E_{\text{inj}} \propto t^{1-q}$  (Zhang et al. 2006), then the energy injection before  $\sim 300$  s is  $\sim 10^{50}$  erg, and we would see an increase in the injected energy by a factor of  $\sim 3$  between 300 and  $10^5$  s. That is, the energy injection from the magnetar wind before  $10^5$  s is at most  $10^{51}$  erg, which is much less than the isotropically equivalent energy of the prompt emission and cannot exceed the initial kinetic energy of the fireball. Therefore, the injected

kinetic energy from the magnetic dipole emission is basically negligible. In the following calculations, we use the energy injection model proposed by Sari & Mészáros (2000) to explain the external plateau of GRB 130831A.

According to Sari & Mészáros (2000), the ejecta are assumed to possess a continuous distribution of Lorentz factors, e.g., the amount of ejected mass moving with Lorentz factors greater than  $\gamma$  is

$$M(>\gamma) \propto \gamma^{-s}, \quad (1)$$

down to some minimum Lorentz factor  $\gamma_{\min} \leq \gamma_0$ , where the initial Lorentz factor  $\gamma_0$  is assumed to be at the deceleration time.  $s > 1$  is required to have a change in the fireball dynamics. The energy of the blastwave increases as  $E \propto \gamma^{(1-s)}$ , and its Lorentz factor  $\gamma \propto t^{[-3/(7+s)]}$  for a homogeneous interstellar medium (ISM) environment which is the case for GRB 130831A (see below).

The evolution of  $E$  can be written as (Laskar et al. 2015)

$$E(t) = \begin{cases} E_i = E_f \left(\frac{t_i}{t_f}\right)^m, & t \leq t_i, \\ E_f \left(\frac{t}{t_f}\right)^m, & t_i < t < t_f, \\ E_f, & t \geq t_f, \end{cases} \quad (2)$$

where  $m = 3(s-1)/(7+s)$  for the ISM case,  $t_i$  and  $t_f$  are the start and end time of the energy injection, respectively; while  $E_i$  and  $E_f$  are the initial and final energy of the blastwave, respectively. For GRB 130831A, the optical plateau starts at around 120 s, so we take  $t_i = 100$  s, which is also assumed to be the deceleration time, and take  $t_f = 5000$  s.

In the following calculations, we adopt  $\alpha_1 = 0.2$  for the plateau decay slope,  $\alpha_2 = 1.59$  for the post-plateau slope and  $\beta_{\text{OX}} = 1.03$  for the spectral index. The closure relations of the post-plateau phase require an ISM environment. The observing frequency should be between the synchrotron peak frequency  $\nu_m$  and the cooling frequency  $\nu_c$ , i.e.,  $\nu_m < \nu_{\text{opt}} < \nu_X < \nu_c$ , and the electron spectral index is derived as  $p = 3.06$  (De Pasquale et al. 2016). Using

the closure relations of the plateau phase (Sari & Mészáros 2000), we obtain  $s = 4.4$ , and  $m = 0.9$ .

We follow the formalism of Gao et al. (2013) to compute the break frequencies and the peak flux ( $\nu_m$ ,  $\nu_c$  and  $F_{\nu, \max}$ ) but replace the blastwave energy with Equation (2) and consider the synchrotron self-Compton (SSC) effect (Sari & Esin 2001). For  $\nu_m < \nu < \nu_c$ , the flux density is

$$F_\nu = 3.5 \mu\text{Jy} E_{52}^{1.52} \epsilon_{e,-1}^{2.06} \epsilon_{B,-2}^{1.02} n_0^{1/2} t_5^{-1.55} \left( \frac{\nu}{\nu_R} \right)^{-1.03}, \quad (3)$$

where  $\nu_R$  is the  $R$ -band frequency,  $E$  is given by Equation (2).

To constrain the parameters, we notice that (i) the  $R$ -band flux at  $t = 19$  ks is  $F_{\nu_R}(19 \text{ ks}) \simeq 0.19 \text{ mJy}^3$ , (ii)  $\nu_c$  should be well above the X-ray band at 2 days, i.e.,  $\nu_c(2 \text{ d}) > 10 \text{ keV}$ , (iii)  $\nu_m$  has crossed the  $V$  band before 120 s, i.e.,  $\nu_m(120 \text{ s}) < \nu_V$ . Then we have

$$E_{f,52}^{1.52} \epsilon_{e,-1}^{2.06} \epsilon_{B,-2}^{1.02} n_0^{1/2} \simeq 4.1, \quad (4)$$

$$E_{f,52}^{-1/2} \epsilon_{B,-2}^{-3/2} n_0^{-1} (1 + Y)^{-2} > 93.6, \quad (5)$$

$$E_{f,52}^{1/2} \epsilon_{e,-1}^2 \epsilon_{B,-2}^{1/2} < 0.7, \quad (6)$$

where  $Y$  is the Compton parameter denoting the energy ratio between the inverse Compton component and the synchrotron component. In the Thomson scattering regime,  $Y = (\eta \epsilon_e / \epsilon_B)^{1/2}$  if  $Y \gg 1$ , while  $Y = \eta \epsilon_e / \epsilon_B$  if  $Y \ll 1$ , where  $\eta = \min \left\{ 1, (\nu_m / \nu_c)^{(p-2)/2} \right\}$  is the fraction of electron energy that was radiated away (Sari & Esin 2001).

---

<sup>3</sup>This value has been corrected for Galactic and host galaxy extinction with  $E(B - V) = 0.04 \text{ mag}$  (Schlegel et al. 1998) and  $E(B - V) = 0.02 \text{ mag}$  (De Pasquale et al. 2016), respectively.

From Equations (4)–(6), one derives

$$E_{f,52} > 48\epsilon_{e,-1}^{-1} (1 + Y), \quad (7)$$

$$\epsilon_{B,-2} < 0.01\epsilon_{e,-1}^{-3} (1 + Y)^{-1}. \quad (8)$$

We simply assume  $E_i = 2E_\gamma = 2.1 \times 10^{52}$  erg. Since we have  $E_f = E_i (t_f/t_i)^{0.9} = 33.8E_i$ , then we get  $E_{f,52} = 71$ . For the other parameters, we take  $\epsilon_{e,-1} = 1$  and  $\epsilon_{B,-2} = 5 \times 10^{-3}$ , then  $n_0 \simeq 2.0$  is obtained from Equation (4). Using these parameters, we check that  $Y < 1$  is satisfied throughout the afterglow stage. Our derived kinetic energy of  $E_f = 7.1 \times 10^{53}$  erg exceeds the usual maximum rotational energy ( $\sim 3 \times 10^{52}$  erg) of a  $1.4 M_\odot$  magnetar. It leads to the doubt that whether such a huge energy can be successfully supplied by the central engine. A very massive magnetar may help to alleviate the difficulty, since the rotational energy could then be up to  $\sim 2 \times 10^{53}$  erg (Metzger et al. 2015). In the case of GRB 130831A, we argue that the beaming effect may be a more realistic choice. When a beaming factor of  $f_b > 7.56 \times 10^{-3}$  (De Pasquale et al. 2016) is considered, the intrinsic kinetic energy will be reduced to  $E_{f,b} > 5.4 \times 10^{51}$  erg, which is compatible with the usual magnetar energy limit.

Using the parameters given above, we can calculate the initial Lorentz factor by  $\gamma_0 \approx 77.5E_{i,52}^{1/8}n_0^{-1/8}t_2^{-3/8}(1+z)^{3/8}$  (Sari et al. 1998), and get  $\gamma_0 \approx 95$ . At the end of the energy injection, the Lorentz factor  $\gamma = \gamma_0 (t_f/t_i)^{-0.26} \approx 34$ , then the ejecta distribution can be described by  $M(>\gamma) \propto \gamma^{-4.4}$ , with  $34 \leq \gamma \leq 95$ .

### 3.2. Afterglow of Internal Origin

According to our fit, the X-ray afterglow LC shows an initial short plateau that lasts for  $\sim 200 - 300$  s, followed by a steeper plateau between 0.3 and 98 ks, then it drops rapidly with a slope of  $\sim 6$ . This steep internal plateau cannot be produced through

the process of dipole spin-down of a magnetar. For a rotating proto-neutron star, strong GW radiation could be produced through some nonaxisymmetric stellar perturbations, such as dynamical instabilities and secular gravitational-wave driven instabilities (see Kokkotas (2008) for a review). The latter are frame-dragging instabilities usually called Chandrasekhar-Friedman-Schutz instabilities (Chandrasekhar 1970; Friedman & Schutz 1978), which is an efficient mechanism for the production of GWs and has a characteristic timescale compatible with the one of the GRB plateaus (Corsi & Mészáros 2009). As stated in Section 1, when the neutron star undergoes GW-driven r-mode instability (Andersson 1998; Friedman & Morsink 1998), GW losses can dominate the spin-down up to  $\sim$  a few  $\times 10^6$  s (Sá & Thomé 2005), so that the relatively steep and long internal X-ray plateau of GRB 130831A can be produced. In the following, we will evaluate the evolution of the magnetic dipole luminosity following the formalism of Yu et al. (2010).

According to a phenomenological second-order model for the r-mode evolution (Owen et al. 1998; Sá 2004), the spin of a magnetar evolves as (Sá 2004; Yu et al. 2009a)

$$\frac{dP}{dt} = \frac{4\bar{\alpha}^2}{15} (\delta + 2) \frac{P}{\tau_g} + \frac{P}{\tau_m}, \quad (9)$$

where  $P$  is the spin period of the magnetar,  $\bar{\alpha}$  is the dimensionless amplitude of the r-modes, and  $\delta$  is a free parameter describing the initial degree of the differential rotation of the star. The gravitational braking timescale can be written as  $\tau_g = 37(P/P_K)^6$  s, where  $P_K$  is the Keplerian period at which the star starts shedding mass at the equator. The magnetic braking timescale is given by  $\tau_m = 4 \times 10^5 I_{45} B_{14}^{-2} P_{-3}^2 R_6^{-6}$  s, where  $I_{45}$  is the moment of inertia in units of  $10^{45}$  g cm<sup>2</sup> and  $R_6$  is the radius of the magnetar in units of  $10^6$  cm. The evolution of the r-mode amplitude  $\bar{\alpha}$  can be calculated from (Sá 2004; Yu et al. 2009a)

$$\frac{d\bar{\alpha}}{dt} = \left[ 1 + \frac{2\bar{\alpha}^2}{15} (\delta + 2) \right] \frac{\bar{\alpha}}{\tau_g} + \frac{\bar{\alpha}}{2\tau_m}. \quad (10)$$

In the case of  $\tau_{g,i} \ll \tau_{m,i}$  (i.e.,  $B \ll B_c = 5 \times 10^{15} P_{i,-3}^{-2}$  G; the subscript “i” of a physical quantity means its initial value here and after), the spin-down would be first dominated by

the gravitational wave radiation. By ignoring the magnetic term, Equations (9) and (10) can be solved analytically, and  $P(t)$  can be described by (Sá & Thomé 2005, 2006)

$$P(t) \approx \begin{cases} P_i \left[ 1 - \frac{2}{15} \bar{\alpha}_i^2 (\delta + 2) \exp(2t/\tau_{g,i}) \right]^{-1}, & \text{for } t < T_g, \\ 1.6 P_i (t/\tau_{g,i})^{1/5}, & \text{for } t > T_g, \end{cases} \quad (11)$$

where the break time  $T_g$  corresponds to the moment when the mode's amplitude changes from an exponential to a much slower power-law growth, and can be solved from  $d^2\bar{\alpha}/dt^2|_{t=T_g} = 0$  to be (Yu et al. 2009b)

$$\begin{aligned} T_g &= -37 \left[ \ln \bar{\alpha}_i + \frac{1}{2} \ln(\delta + 2) + \frac{1}{2} \ln\left(\frac{6}{5}\right) \right] \left( \frac{P_i}{P_K} \right)^6 \\ &\equiv T_K(\bar{\alpha}_i, \delta) \left( \frac{P_i}{P_K} \right)^6. \end{aligned} \quad (12)$$

Within a wide parameter region of  $10^{-10} < \bar{\alpha}_i < 10^{-6}$  and  $0 < \delta < 10^8$ ,  $T_K$  varies from 170 to 840 s (Sá & Thomé 2005, 2006; Yu et al. 2009b). As the spin period increases, the magnetic braking effect would eventually exceed the gravitational braking effect and then  $P$  evolves from  $P \propto t^{1/5}$  to  $P \propto t^{1/2}$ . The transition happens at  $T_c$  given below.

We can calculate the magnetic dipole luminosity of a magnetar by (Yu et al. 2010)

$$L_{\text{md}}(t) = 10^{47} F(t) B_{14}^2 P_{i,-3}^{-4} R_6^6 \text{ erg s}^{-1}, \quad (13)$$

where for  $B < B_c$ ,

$$F(t) \approx \begin{cases} t^0, & t < T_g, \\ \left( \frac{t}{T_g} \right)^{-q}, & T_g < t < T_c, \\ \left( \frac{T_c}{T_g} \right)^{-q} \left( \frac{t}{T_c} \right)^{-2}, & t > T_c. \end{cases} \quad (14)$$

Here  $T_c = (T_m^2/T_g^q)^{1/(2-q)}$  corresponds to the transition time when the magnetic braking effect exceeds the gravitational braking effect, and  $T_m = 2 \times 10^5 I_{45} B_{14}^{-2} P_{i,-3}^2 R_6^{-6}$  s is the initial spin-down timescale. According to Equation (11),  $q$  can be taken as 0.8 approximately.



We note that the magnetic dipole emission does not convert completely into X-rays. By considering the converting effect and the correction for the beaming of the magnetar wind, we can write the observed X-ray luminosity as

$$L_X = \eta_X L_{\text{md}} / f_b = 10^{47} \eta_{X,-1} f_{b,-1}^{-1} L_{\text{md},47} \text{ erg s}^{-1}, \quad (15)$$

where  $\eta_X$  and  $f_b$  are the efficiency in converting the magnetic dipole emission into X-ray radiation and the beaming factor of the magnetar wind, respectively.

For GRB 130831A, however, we revise this scenario by requiring the magnetar collapses into a black hole well before  $T_c$  to explain the sharp drop of the X-ray LC at about  $10^5$  s. To constrain the parameters, we require: (i)  $(1+z)T_g \simeq 269$  s, (ii) the initial plateau luminosity  $L_X \simeq 2.6 \times 10^{47} \text{ erg s}^{-1}$ , (iii)  $(1+z)T_c > 9.8 \times 10^4$  s. We assume  $T_K = 170$  s and  $\eta_X/f_b = 1$ , then following the expressions of  $T_g$ ,  $T_c$  and Equations (13)–(15), we obtain the initial spin period  $P_i \simeq 1.01 P_K$  and the magnetic field strength  $B_{14} \simeq 1.0$ . We note that our obtained spin period is very close to the Keplerian period (i.e., the minimum spin period allowed before breakup), which can be taken as 0.8 ms for a  $1.4 M_\odot$  neutron star (Lattimer & Prikash 2004; Haensel et al. 2009).

#### 4. COMPARISON WITH OBSERVED LIGHT CURVES

We have calculated the theoretical multi-band afterglow LCs based on Equations (2), (3), (13)–(15) and on our derived parameters in Section 3. For the decay slope after the magnetar collapses into a black hole, we artificially set it as 6.8 according to the fitting results of De Pasquale et al. (2016).

Figure 3 compares our theoretical 0.3 – 10 keV LC with the X-ray flux observed by XRT and *Chandra*. It is shown that our model can basically describe the observed flux evolution. We note, however, our model slightly overestimates the internal plateau. This

is because we use the plateau decay index of 0.8 following Equations (11) and (14) which are solved analytically, a slightly larger value ( $\sim 1$ ) can be obtained from a more accurate numerical calculation (Yu et al. 2010), which would improve the modeling. Moreover, the external afterglow has a small contribution to the internal X-ray plateau. In addition, the theoretical X-ray flux underestimates the late XRT and *Chandra* data points except for the last one which has very large errors. This is to be expected, since the theoretically predicted decay index of the FS component is 1.55, which is slightly steeper than the observed value ( $\sim 1.1$ ). However, when the uncertainties are considered, they are consistent at  $2.1\sigma$  CL (De Pasquale et al. 2016). For the multi-band optical afterglow plot in Figure 4, our model also gives a good explanation except for the *U* band data, which show a slight excess between 200 and 500 s. The reason may be that the energy injection model adopted here is still too simplified. More realistic and complicated external shock processes might be involved and need further investigations.

Another possibility is that the magnetar wind emission may have a significant contribution to the initial optical plateau. According to our magnetar model and our fitting results of the X-ray afterglow, the wind emission could produce a short X-ray plateau lasting for  $\sim 300$  s, which is compatible with the timescale of the early optical plateau. To check the flux level, we assume that the magnetar wind emission can extend to the optical band with the spectral index  $\beta_X = 0.77 \pm 0.07$ , then extrapolate the flux density of the initial X-ray plateau to the optical band using the fitted flux parameters (see Table 1), and compare with the early data in the *U* and *V* bands. As shown in Figure 5, the predicted initial optical plateau is now in accord with the *V* band data rather well, and it is also consistent with the *U* band data at  $1\sigma$  CL. In this case, even the energy injection from the refreshed shocks is no longer needed for this short period. The optical afterglow after  $\sim 3$  ks can be interpreted in the context of the standard afterglow model, and the late plateau (between  $\sim 3$  and 5 ks) is produced by the superposition of a decaying optical flare

and a rising FS peak (De Pasquale et al. 2016). However, to avoid exceeding the external component at late times ( $\sim 100$  ks), we have to assume that the internal optical emission fade rapidly at some time. Moreover, according to this explanation, the flux before and after the flare have roughly the same normalization but with completely different origins, which makes this scenario somewhat contrived.

## 5. CONCLUSIONS AND DISCUSSIONS

The X-ray afterglow of GRB 130831A shows a shallow decay followed by a steep drop at about  $10^5$  s, which is the signature of an “internal plateau”. After the drop, the X-ray afterglow continues with a much shallower decay, a similar decay behavior appears in the optical afterglow after  $\sim 5$  ks. Before  $\sim 5$  ks, the optical afterglow shows two segments of plateaus separated by a pronounced optical flare peaking at  $\sim 730$  s. The decay slope of the internal X-ray plateau ( $\sim 0.8$ ) is so steep that it cannot be explained by the simplest magnetar spin-down model. We interpret this special internal plateau as the magnetar wind emission during the spin-down process dominated by GW radiation losses in the context of r-mode instability, and explain the steep drop by assuming that the magnetar collapses into a black hole. This scenario also predicts an initial X-ray plateau lasting for hundreds of seconds which is compatible with observations. By assuming that the two segments of optical plateaus have the same external origin and the magnetar wind emission has a negligible contribution in the optical band, we interpret the optical and late X-ray afterglow as FS emission by invoking the energy injection from a continuously refreshed shock following the prompt emission phase. It is shown that the U-band afterglow has a slight excess before  $\sim 500$ s. One possibility is that our analytical treatment of the energy injection model is still too simplified and more complicated external shock processes might be called for. Another solution is that the magnetar wind emission might have a significant

contribution to the early optical afterglow.

The observed X-ray internal plateaus are typically flat and can be produced through the spin-down process caused by dipolar radiation before the magnetar collapses into a black hole. About 29–56% short GRBs exhibit an internal plateau (Rowlinson et al. 2013; Lü et al. 2015; Gao et al. 2016), whereas this is much lower for long GRBs (10 candidates identified in Lyons et al. 2010). The magnetic field strength and spin period required to reproduce the observed internal plateaus in both long and short GRBs are typically  $P_i \sim 1 - 10$  ms and  $B \sim 10^{15} - 10^{16}$  G (Lyons et al. 2010; Rowlinson et al. 2013; Lü et al. 2015). For GRB 130831A, our derived parameters of  $P_i \simeq 0.8$  ms and  $B \simeq 10^{14}$  G are at the lower end of these distributions. This is not surprising, however, since the internal plateau of this burst is quite different from those usually studied. In our magnetar model, the extreme spin period is solely determined by the break time  $T_g \sim 270$  s, while the weak magnetic field strength is determined by the luminosity of the X-ray initial plateau. Besides, such a weak magnetic field strength is also required by the long duration of the internal plateau of GRB 130831A. To produce this plateau, the GW losses would dominate the spin-down until  $\sim 10^5$  s (i.e.,  $(1+z)T_c > 10^5$  s), which gives  $B_{14} < 4$ . Therefore, it is the unique feature of the internal plateau of GRB 130831A that determines the extreme spin period and magnetic field strength.

In our magnetar scenario, the magnetic dipole radiation is strong and significant up to  $\sim 100$  ks, and it can successfully power the internal X-ray plateau. It is assumed that this dipole radiation component mainly contributes to the emission in X-ray band, but contribute negligibly at optical wavelengths. To interpret the optical plateau that lasts for  $\sim 5$  ks in the case of GRB 130831A, we invoke the energy injection from a continuously refreshed shock following the prompt emission phase. We would like to stress that the hypothesis that the magnetic dipole radiation mainly contributes to X-ray emission but

not optical emission is still an assumption. It needs to be further checked by future observations. Interestingly, it seems that the assumption already received some support from observations. Previous studies have indicated that the magnetar wind emission tends to contribute to the internal plateau mostly in X-rays, but it is usually not detected at optical bands (Troja et al. 2007; Lyons et al. 2010; Rowlinson et al. 2013). Rowlinson et al. (2013) found that several short GRBs with internal plateaus have optical afterglows which are consistent with their X-ray afterglows during the plateau phase, but these cases would require some extreme parameters. Therefore, whether the magnetar wind emission produces the internal plateau in the optical band is not conclusive in their analysis.

To produce the multi-band afterglow of GRB 130831A, our model invokes two different outflow components. One is an “active” outflow, which internally produces X-ray emission for  $\sim 100$  ks. The other outflow, instead, does not produce internal emission, but still increases the energy of the leading ejecta for  $\sim 5$  ks, leading to the observed optical plateau. This scenario is somewhat more complicated as compared with many previous GRB scenarios in which usually only one component is involved. Since the multi-band afterglow behavior of GRB 130831A itself is very complicated, we believe that such a choice is still reasonable. We argue that in our scheme, the external and internal plateaus may coexist in the multi-band afterglow. It can be tested by more similar observations in the future.

We acknowledge the anonymous referee for helpful comments and suggestions. This work made use of data supplied by the UK Swift Science Data Centre at the University of Leicester. Our study was supported by the National Basic Research Program of China with Grant No. 2014CB845800 and by the National Natural Science Foundation of China with Grants No. 11473012, No. 11475085, and No. 11275097.

## REFERENCES

- Andersson, N. 1998, *ApJ*, 502, 708
- Band, D., Matteson, J., Ford, L., et al. 1993, *ApJ*, 413, 281
- Barthelmy, S. D., Barbier, L. M., Cummings, J. R., et al. 2005, *SSRv*, 120, 143
- Bucciantini, N., Metzger, B. D., Thompson, T. A., & Quataert, E. 2012, *MNRAS*, 419, 1537
- Burrows, D. N., Hill, J. E., Nousek, J. A., et al. 2005, *SSRv*, 120, 165
- Butler, N., Klein, C., Fox, O., et al. 2012, *SPIE*, 8446, 10
- Cano, Z., De Ugarte Postigo, A., Pozanenko, A., et al. 2014, *A&A*, 568, 19
- Chandrasekhar, S. 1970, *PhRvL*, 24, 611
- Chevalier, R. A., & Li, Z. Y. 2000, *ApJ*, 536, 195
- Chincarini, G., Mao, J., Margutti, R., et al. 2010, *MNRAS*, 406, 2113
- Corsi, A., & Mészáros, P. 2009, *ApJ*, 702, 1171
- Cucchiara, A., & Perley, D. 2013, *GCN*, 15144, 1
- Dai, Z. G., & Lu, T. 1998, *A&A*, 333, L87
- De Pasquale, M., Oates, S. R., Racusin, J. L., et al. 2016, *MNRAS*, 455, 1027
- Eichler, D., & Granot, J. 2006, *ApJL*, 641, L5
- Evans, P. A., Beardmore, A. P., Page, K. L., et al. 2007, *A&A*, 469, 379
- Evans, P. A., Beardmore, A. P., Page, K. L., et al. 2009, *MNRAS*, 397, 1177
- Falcone, A. D., Morris, D., Racusin, J. L., et al. 2007, *ApJ*, 671, 1921

- Friedman, J. L., & Morsink, S. M. 1998, *ApJ*, 502, 714
- Friedman, J. L., & Schutz, B. F. 1978, *ApJ*, 222, 281
- Gao, H., Lei, W. H., Zou, Y. C., Wu, X. F., & Zhang, B. 2013, *NewAR*, 57, 141
- Gao, H., Zhang, B., & Lü, H. J. 2016, *PhRvD*, 93, 044065
- Gehrels, N., Chincarini, G., Giommi, P., et al. 2004, *ApJ*, 611, 1005
- Ghisellini, G., Ghirlanda, G., Nava, L., & Firmani, C. 2007, *ApJL*, 658, L75
- Golenetskii, S., Aptekar, R., Fredericks, D. A., et al. 2013, *GCN*, 15145, 1
- Grupe, D., Nousek, J. A., Veres, P., Zhang, B. B., & Gehrels, N. 2013, *ApJS*, 209, 20
- Haensel, P., Zdunik, J. L., Bejger, M., & Lattimer, J. M. 2009, *A&A*, 502, 605
- Hagen, L. M. Z., Chester, M. M., Cummings, J. R., et al. 2013, *GCN*, 15139, 1
- Huang, Y. F., Dai, Z. G., & Lu, T. 1999, *MNRAS*, 309, 513
- Ioka, K., Toma, K., Yamazaki, R., & Nakamura, N. 2006, *A&A*, 458, 7
- Jarosik, N., Bennet, C. L., Dunkley, J., et al. 2011, *ApJS*, 192, 14
- Kokkotas, K. D. 2008, *RvMA*, 20, 140
- Kumar, P., & Zhang, B. 2015, *PhR*, 561, 1
- Laskar, T., Berger, E., Margutti, R., et al. 2015, *ApJ*, 814, 1
- Lattimer, J. M., & Prakash, M. 2004, *Sci*, 304, 536
- Lei, W. H., Zhang, B., & Liang, E. W. 2013, *ApJ*, 765, 125
- Liang, E. W., Zhang, B. B., & Zhang, B. 2007, *ApJ*, 670, 565

- Lü, H. J., & Zhang, B. 2014, *ApJ*, 785, 74
- Lü, H. J., Zhang, B., Lei, W. H., & Lasky, P. D. 2015, *ApJ*, 805, 89
- Lyons, N., O’Brien, P. T., Zhang, B., et al. 2010, *MNRAS*, 402, 705
- Margutti, R., Bernardini, G., Barniol Duran, R., et al. 2011, *MNRAS*, 410, 1064
- Margutti, R., Zaninoni, E., Bernardini, M. G., et al. 2013, *MNRAS*, 428, 729
- Mészáros, P., & Rees, M. J. 1993, *ApJ*, 405, 278
- Mészáros, P., & Rees, M. J. 1997, *ApJ*, 476, 232
- Metzger, B. D., Giannios, D., Thompson, T. A., et al. 2011, *MNRAS*, 413, 2031
- Metzger, B. D., Quataert, E., & Thompson, T. A. 2008, *MNRAS*, 385, 1455
- Metzger, B. D., Margalit, B., Kasen, D., & Quataert, E. 2015, *MNRAS*, 454, 3311
- Molotov, I., Agapov, V., Titenko, V. D., et al. 2008, *AdSpR*, 41, 1022
- Narayan, R., Piran, T., & Kumar, P. 2001, *ApJ*, 557, 949
- Nousek, J. A., Kouveliotou, C., Grupe, D., et al. 2006, *ApJ*, 642, 389
- O’Brien, P. T., Willingale, R., Osborne, J., et al. 2006, *ApJ*, 647, 1213
- Owen, B. J., Lindblom, L., Cutler, C., et al. 1998, *PhRvD*, 58, 084020
- Popham, R., Woosley, S. E., & Fryer, C. 1999, *ApJ*, 518, 356
- Pozanenko, A., Elenin, L., Litvinenko, E., et al. 2013, *EAS*, 61, 259
- Racusin, J. L., Liang, E. W., Burrows, D. N., et al. 2009, *ApJ*, 698, 43
- Rees, M. J., & Mészáros, P. 1992, *MNRAS*, 258, 41



- Rees, M. J., & Mészáros, P. 1998, *ApJL*, 496, L1
- Reichart, D., Nysewander, M., Moran, J., et al. 2005, *NCimC*, 28, 767
- Roming, P. W. A., Kennedy, T. E., Mason, K. O., et al. 2005, *SSRv*, 120, 95
- Rowlinson, A., O’Brien, P. T., Metzger, B. D., et al. 2013, *MNRAS*, 430, 1061
- Rowlinson, A., O’Brien, P. T., Tanvir, N. R., et al. 2010, *MNRAS*, 409, 531
- Sá, P. M. 2004, *PhRvD*, 69, 084001
- Sá, P. M., & Thomé, B. 2005, *PhRvD*, 71, 044007
- Sá, P. M., & Thomé, B. 2006, *PhRvD*, 74, 044011
- Sari, R., & Esin, A. A. 2001, *ApJ*, 548, 787
- Sari, R., & Mészáros, P. 2000, *ApJL*, 535, L33
- Sari, R., Piran, T., & Narayan, R. 1998, *ApJL*, 497, L17
- Schlegel, D. J., Finkbeiner, D. P., & Davis, M., 1998, *ApJ*, 500, 525
- Shao, L., & Dai, Z. G. 2007, *ApJ*, 660, 1319
- Thompson, C. 1994, *MNRAS*, 270, 480
- Troja, E., Cusumano, G., O’Brien, P. T., et al. 2007, *ApJ*, 665, 599
- Uhm, Z. L., & Beloborodov, A. M. 2007, *ApJL*, 665, L93
- Usov, V. V. 1992, *Natur*, 357, 472
- Wheeler, J. C., Yi, I., Höflich, P., & Wang, L. 2000, *ApJ*, 537, 810
- Yu, Y. W., Cao, X. F., & Zheng, X. P. 2009a, *RAA*, 9, 1024

Yu, Y. W., Cao, X. F., & Zheng, X. P. 2009b, *ApJL*, 706, L221

Yu, Y. W., Cheng, K. S., & Cao, X. F. 2010, *ApJ*, 715, 477

Zhang, B. 2014, *ApJL*, 780, L21

Zhang, B., Fan, Y. Z., Dyks, J., et al. 2006, *ApJ*, 642, 354

Zhang, B., & Mészáros, P. 2001, *ApJL*, 552, L35

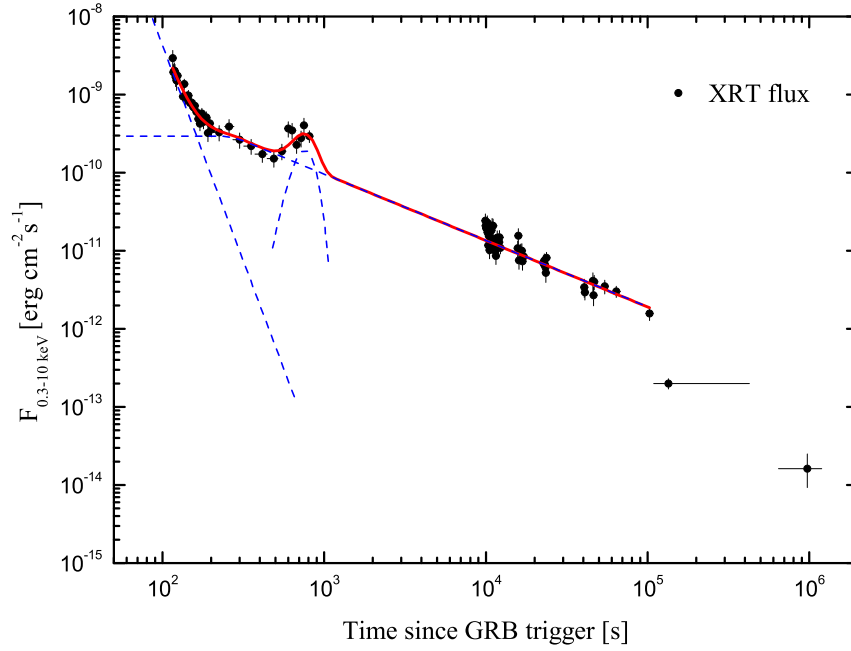


Fig. 1.— Fit of the X-ray flux of GRB 130831A with the PL+BPL+Gauss model (solid line). The data are taken from [http://www.swift.ac.uk/burst\\_analyser/00568849/](http://www.swift.ac.uk/burst_analyser/00568849/) (Evans et al. 2009). The three fitting components (dashed lines) are displayed for clarity.

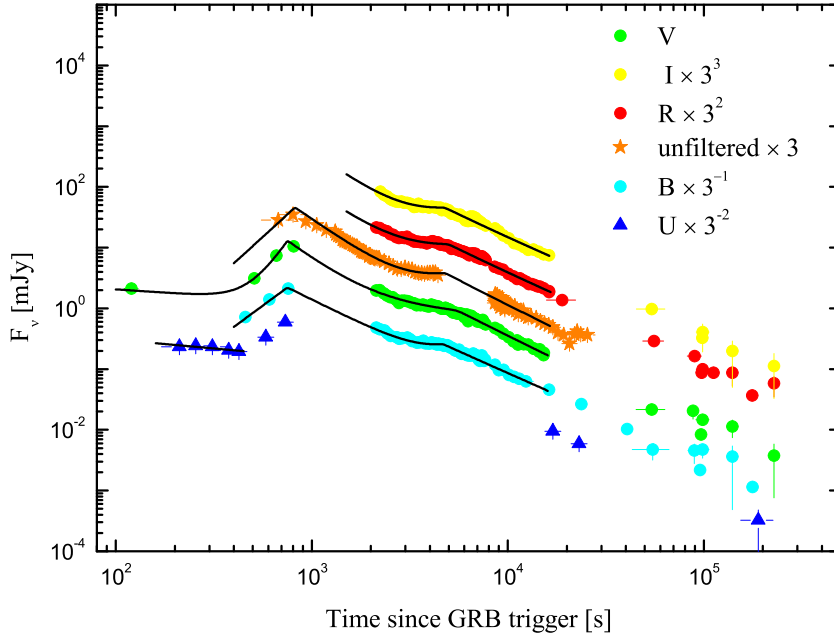


Fig. 2.— Fit of the optical light curves of GRB 130831A before 16 ks (solid lines). The  $V$ ,  $B$  and unfiltered bands are fitted with two BPLs, while the  $R$  and  $I$  bands are fitted with a PL+BPL. For the  $U$  band, we fit only the initial plateau with a PL. The data are taken from De Pasquale et al. (2016). Adjacent light curves have been offset by a factor of three for clarity, with  $V$  band unscaled.

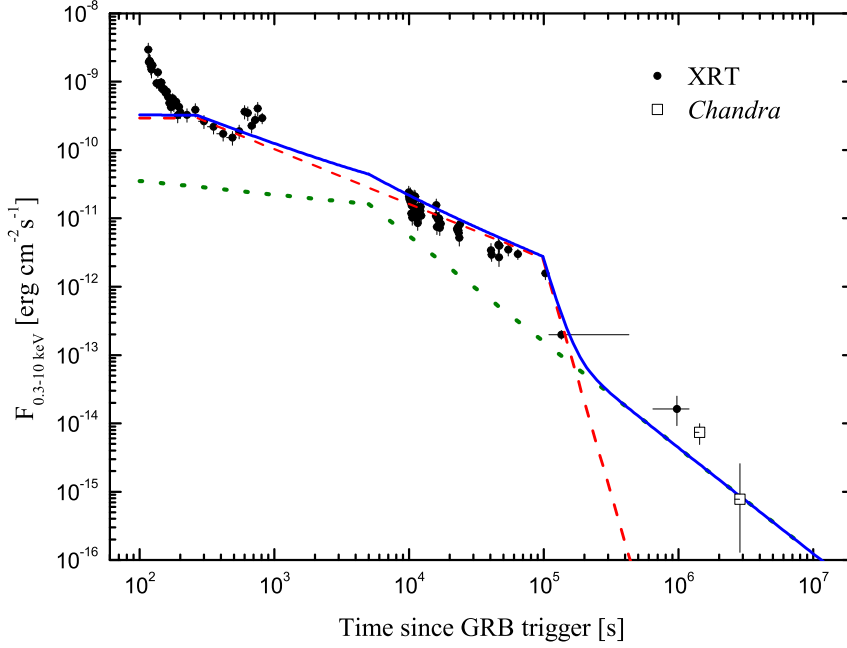


Fig. 3.— Our theoretical X-ray afterglow light curves as compared with the observed X-ray flux of GRB 130831A. The parameter values of  $\epsilon_{e,-1} = 1$ ,  $\epsilon_{B,-2} = 5 \times 10^{-3}$ ,  $E_{f,52} = 71$ ,  $n_0 = 2.0$ ,  $P_{i,-3} = 0.8$  and  $B_{14} = 1.0$  are used. The XRT data (dots) are taken from [http://www.swift.ac.uk/burst\\_analyser/00568849/](http://www.swift.ac.uk/burst_analyser/00568849/) (Evans et al. 2009). The *Chandra* data (squares) are taken from De Pasquale et al. (2016). The dotted and dashed lines correspond to calculated external and internal afterglow components, respectively. The solid line is the superposition of both components. The initial steep decay and X-ray flare are not considered.

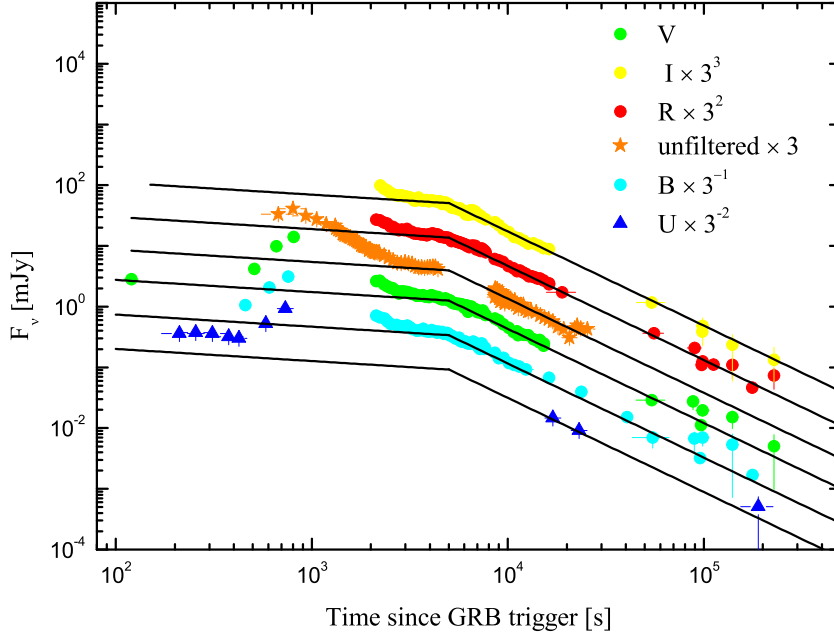


Fig. 4.— Our theoretical multi-band optical afterglow light curves as compared with the observations of GRB 130831A. The parameter values of  $\epsilon_{e,-1} = 1$ ,  $\epsilon_{B,-2} = 5 \times 10^{-3}$ ,  $E_{f,52} = 71$ ,  $n_0 = 2.0$  are used. The predicted emissions are from the FS (solid lines). The data are taken from De Pasquale et al. (2016) and have been corrected for Galactic and host galaxy extinction. Adjacent light curves have been offset by a factor of three for clarity, with  $V$  band unscaled. The optical flares are not considered.

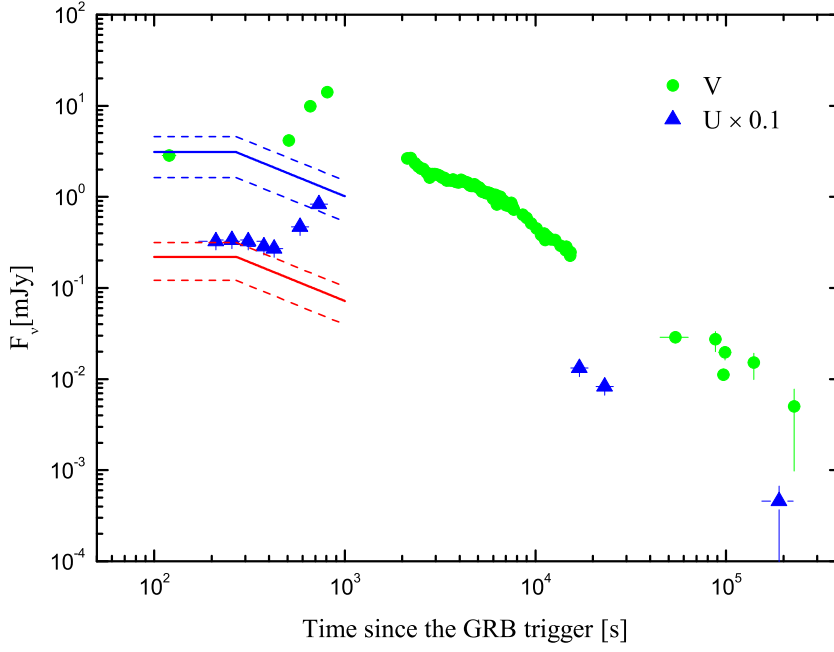


Fig. 5.— Predicted  $U$  and  $V$  band afterglow (solid lines) from the magnetar wind internal emission as compared with the observed early afterglow. The dashed lines correspond to the  $1\sigma$  CL. The data are taken from De Pasquale et al. (2016) and have been corrected for Galactic and host galaxy extinction. The  $U$  band data have been rescaled by a factor of 0.1 for clarity.

Table 1. Fitting parameters of the X-ray afterglow before  $10^5$  s.

| Model           | $\alpha_{\text{PL}}$ | $f_0$<br>( $\times 10^{-10}$ erg cm $^{-2}$ s $^{-1}$ ) | $\alpha_1$ | $t_b$<br>(s) | $\alpha_2$      | $f_1$<br>( $\times 10^{-10}$ erg cm $^{-2}$ s $^{-1}$ ) | $t_c$<br>(s) | $w$<br>(s)   | $\chi^2/dof$ |
|-----------------|----------------------|---|------------|--------------|-----------------|---|--------------|--------------|--------------|
| PL+BPL+Gaussian | $5.52 \pm 0.92$      | $2.93 \pm 0.62$   | 0 (fixed)  | $269 \pm 75$ | $0.85 \pm 0.02$ | $1.94 \pm 0.37$   | $760 \pm 47$ | $165 \pm 66$ | 76/80        |

Note. — The fitting functions are: (a) a PL with the decay index  $\alpha_{\text{PL}}$ ; (b) a BPL with the decay indices  $\alpha_1$ ,  $\alpha_2$ , break time  $t_b$  and flux normalisation  $f_0$ , we fix  $\alpha_1 = 0$ ; (c) a Gaussian function presented by  $f = f_1 \exp[-(t - t_c)^2/w^2]$ .



Table 2. Fitting parameters of the optical afterglow before 16 ks.

| Filter     | $\alpha_1$       | $t_b$<br>(ks)   | $\alpha_2$      | $\alpha_1^F$   | $t_b^F$<br>(ks) | $\alpha_2^F$  | $\chi^2/dof$ |
|------------|------------------|-----------------|-----------------|----------------|-----------------|---------------|--------------|
| <i>V</i>   | $0.22 \pm 0.06$  | $5.51 \pm 0.14$ | $1.55 \pm 0.04$ | $-4.9 \pm 1.2$ | $0.75 \pm 0.03$ | $2.5 \pm 0.1$ | 254/74       |
| <i>B</i>   | $-1.79 \pm 0.62$ | $4.66 \pm 0.11$ | $1.32 \pm 0.06$ | $-2.4 \pm 0.2$ | 0.75 (fixed)    | $1.6 \pm 0.1$ | 105/62       |
| unfiltered | $-0.97 \pm 0.37$ | $4.77 \pm 0.17$ | $1.51 \pm 0.08$ | -3 (fixed)     | $0.81 \pm 0.02$ | $2.2 \pm 0.1$ | 197/99       |
| <i>R</i>   | $-0.47 \pm 0.17$ | $4.96 \pm 0.10$ | $1.40 \pm 0.03$ |                |                 | 2.3 (fixed)   | 284/74       |
| <i>I</i>   | $-0.79 \pm 0.27$ | $4.75 \pm 0.11$ | $1.35 \pm 0.05$ |                |                 | 2.3 (fixed)   | 208/65       |
| <i>U</i>   | $0.29 \pm 0.10$  |                 |                 |                |                 |               | 8/3          |

Note. — The *V*, *B* and unfiltered bands are fitted with two BPLs, while the *R* and *I* bands are fitted with a PL+BPL. For the *U* band, we fit only the initial plateau with a PL. The temporal parameters of the plateau components are  $\alpha_1$ ,  $\alpha_2$  and  $t_b$ , while those with the superscript “F” correspond to the optical flares.